Journal of the European Ceramic Society 22 (2002) 1543–1552

www.elsevier.com/locate/jeurceramsoc

Comparison of different alumina powders for the aqueous processing and pressureless sintering of Al_2O_3–SiC nanocomposites

B. Baron, C.S. Kumar, G. Le Gonidec, S. Hampshire*

Materials and Surface Science Institute, University of Limerick, Limerick, Ireland

Received 30 August 2000; received in revised form 18 August 2001; accepted 19 September 2001

Abstract

Four different alumina powders, from European and Japanese sources having similar particle size (350–700 nm) were used for the fabrication of nanocomposites. They were compared in terms of green properties, sintering behaviour, microstructure and mechanical properties. The processing route used (attrition milling and freeze-drying) leads to a reduction in green density of the processed aluminas and composites compared to the as-received alumina. All powders had similar green properties except one, which contained a binder from the manufacturer. The presence of this binder led to the formation of hard agglomerates. In this case the pressing did not eliminate, totally, the inter-agglomerate pores, leading to an incomplete sintering. Calcining the powder to remove the binder resulted in similar pressing and sintering behaviour to the other powders and densities >99% were achieved at 1750 °C by pressureless sintering. All the composites exhibited similar microstructures (matrix grain size ~3 μm) and elastic properties, hardness and fracture toughness. A finer matrix microstructure could be obtained with one of the European powders which achieved ~99% density at 1700 °C. The presence of 5 vol.% SiC resulted in a mean grain size of ~2 μm for the alumina matrix compared with 13.9 μm for a monolithic alumina prepared under identical conditions.

Keywords: Al_2O_3–SiC; Green properties; Microstructure-prefiring; Mercury porosimetry; Nanocomposites; Sintering

1. Introduction

The concept of structural ceramic nanocomposites was first proposed by Niihara.[1,2] Within these types of materials, the Al_2O_3–SiC system has been the focus of many studies conducted by different research groups.[1–10] These composites have been reported to exhibit high fracture strengths of over 1000 MPa up to 1000 °C, with improved toughness and creep resistance.[11–13] Recent developments have also shown an improvement of 2–3 times in the wear resistance of Al_2O_3–SiC nanocomposites compared to monolithic alumina of the same grain size.[7,9] These nanocomposites could, thus, represent an interesting alternative for wear resistance applications in terms of cost and performance, lying between alumina and more technical ceramics such as silicon carbide or silicon nitride. In this context, efforts have been made to develop new more commercially viable fabrication routes based on water processing and pressureless sintering.[7] Nearly fully dense (99.6%) materials containing 5 vol.% of SiC were obtained by pressureless sintering, at 1775 °C for 4 h, a powder mixture prepared by attrition milling in water followed by freeze-drying.[10]

In this work, a similar approach has been used for the fabrication of nanocomposites using four different commercial alumina powders and adding 5 vol.% of SiC particles (20–200 nm). The green properties and sintering behaviour of these materials are compared and discussed. The microstructures and mechanical properties are assessed.

2. Experimental procedure

2.1. Starting materials

Four different α-alumina powders and one silicon carbide powder were used for this study. Their characteristics are summarised in Table 1. AES11C (Sumitomo), P172SB (Pechiney) and CS400M (Martinswerk) are commercially available while R/CCC is a laboratory grade alumina

* Corresponding author.
E-mail address: stuart.hampshire@ul.ie (S. Hampshire).

0955-2219/02/$ - see front matter
PII: S0955-2219(01)00467-8

Table 1
Particle size and specific surface area and impurities of the powders used (as given by the manufacturers)

Raw materials	Grade	Mean particle size, d_{50} (nm)	Specific surface area (m^2/g)	Impurities (wt.%)			
				SiO_2	MgO	Na_2O	Other
Al_2O_3 (Sumitomo)	AES11C	400	7–8	0.07	0.00	0.07	Fe_2O_3, CaO, B_2O_3
Al_2O_3 (Pechiney)	P172SB	500	9–10	0.1	0.04	0.08	CaO, B_2O_3, Fe_2O_3
Al_2O_3 (Martinswerk)	CS400M	600–700	12–13	0.06	0.002	0.10	CaO, B_2O_3, Fe_2O_3
Al_2O_3 (Treibacher)	R/CCC	350–450	21	0.15–0.30	0.15–0.20	<0.1	CaO, TiO_2
SiC (HC Starck)	UF45	20–200	44	Free C (0.58), free Si (0.22), Al (0.03), O (3.5)			

received from Treibacher Schleifmittel (Korund Laufenburg Gmbh, Germany). The as-received R/CCC powder was spray-dried and contained a binder ($\sim$3 wt.% PVA). The SiC used was H.C. Starck UF 45 (α-SiC) with particle size ranging from 20 to 200 nm (manufacturer's data).

2.2. Mixing of the alumina and SiC powders

The alumina and silicon carbide powders were mixed by attrition milling in distilled water (Si_3N_4 container and milling media) at a speed of 1000 rpm for 2 h. The isoelectric point of the alumina powders was in the range 9–10.5 and that of SiC was 3.[7,14] Hence, the pH of the slurry was set to a value >11.5 using ammonium hydroxide solution. This corresponds to a zeta potential lower than -25 mV for all the powders, which is necessary for a good dispersion. A dispersant (0.4 wt.% of Darvan C) was added to the slurry in order to improve further the quality of the dispersion. The slurries were then dried using freeze-drying (Edwards Modulyo 4K Freeze Dryer). A typical batch contained 70 g of composite powder.

2.3. Preparation of green compacts

Green compacts were prepared by uniaxial pressing, cold isostatic pressing or by a combination of the two techniques. Pressing pressures in the range 50–250 MPa were used. Uniaxial pressing was conducted using a Lloyd 50 K testing machine in order to obtain accurate and reproducible pressing conditions. Compacts were prepared from the as-received alumina powders, processed alumina powders and the alumina–SiC mixtures. The influence of several parameters (processing, pressing pressure, nature of the alumina powder, presence of SiC) on the green properties of these materials were studied.

2.4. Fabrication and pressureless sintering conditions

The samples used for the mercury porosimetry study were prepared by cold isostatic pressing of the as-received and processed powders at 50 MPa. They were sintered in an alumina tube furnace for 1 h at 1200, 1400 and 1600 °C under a flowing nitrogen atmosphere using an alumina crucible and a SiC powder bed (grit 400). The heating rate was 3 °C/min.

For the rest of the sintering study, the freeze-dried powders were sieved (150 μm) and green samples were prepared by cold isostatic pressing at 150 MPa. The pellets were fired in a graphite element furnace, in a closed graphite crucible, with a SiC powder bed (grit 400) and a flowing nitrogen atmosphere. The samples were sintered at temperatures between 1600 and 1750 °C for 2 h using a heating rate of 5 °C/min.

Following initial sintering and studies of the resulting pore structure, samples prepared from R/CCC were calcined at 600 °C/6 h in air before sintering in order to burn-out the binder.

3. Characterisation techniques

The green compacts were characterised by measuring their green density, green strength and for some of them, by measuring their pore size distribution. The green densities were calculated by measurement of the dimensions of the uniaxialy pressed pellets and using a geopycnometer (Geopyc 1360, Micromeretics) for the cold isostatically pressed compacts. The green strength was measured on pellets (8 mm diameter and height) prepared by uniaxial pressing (50–250 MPa) or uniaxial pressing (50 MPa) followed by cold isostatic pressing (50–200 MPa). Compression tests were conducted using an Instron 4562 testing machine and a cross-head speed of 5 mm/min.

Mercury porosimetry (Quantachrom porosimeter) was used for the characterisation of the pore structure of green and partially sintered samples. When a binder was present, the compacts were calcined prior to measurement. The samples used had a weight of about 1.5 g.

The density of the sintered samples was measured by the Archimedes method in water. The theoretical density of Al_2O_3–5 vol.% SiC nanocomposite (3.94 g/cm^3) was calculated assuming a density of 3.98 g/cm^3 for Al_2O_3 and 3.20 g/cm^3 for SiC.

The microstructural study was conducted on polished and etched surfaces using scanning electron microscopy

(Jeol 840). All the samples having densities above 99% theoretical were characterised. Samples were thermally etched at 1400 °C for 1 h using argon atmosphere, in order to reveal the grain boundaries. The grain size was evaluated using the lineal intercept method.[15] A minimum of 250 Al_2O_3 grains from 5 randomly selected areas were counted for each sample.

Young's and shear moduli were determined by means of an ultrasonic technique, with 10 MHz piezoelectric transducers. E and G were calculated from the following equations:

$$E = \rho\left(3V_l^2 - 4V_t^2\right)/\left(V_l^2/V_t^2 - 1\right) \quad (1)$$

$$G = \rho V_t^2 \quad (2)$$

where ρ is the the density, V_l is the longitudinal wave velocity and V_t is the transversal wave velocity. Poisson's ratio was then calculated from :

$$\nu = (E/2G) - 1 \quad (3)$$

The accuracy of the results obtained here was estimated at ± 2 GPa.

Hardness and fracture toughness were measured by means of Vickers indentation method. A load of 10 kg was applied for 30 s. The hardness (in Pa) was calculated from the following formula:

$$H = 1.8544\frac{P}{(2a)^2} \quad (4)$$

where P (N) is the applied load and $2a$ (m) the diagonal of the indent. The mode 1 fracture toughness (K_{IC}) was calculated from the measurement of the length of the cracks using the Evans and Charles[16] equation:

$$K_{IC} = 0.057H^{0.6}E^{0.4}a^2c^{-1.5} \quad (5)$$

where E is the Young's modulus and c is half of the total crack span.

4. Results and discussion

4.1. Green properties

Preliminary investigations have shown that the addition of 5 vol.% of SiC had no significant effect on the green properties and on the pore size distribution of the alumina compacts. This was expected due to the low amount of SiC and to its relatively small difference in particle size compared to the alumina powders used for this study. The comparison of the green properties was thus conducted only on alumina powders.

The four alumina powders had similar particle sizes and hence should have similar green properties. Table 2 shows, from measurements of green density and strength, that this assumption is valid, with the exception of R/CCC, which contained a binder. For comparison purposes, compacts were also prepared from a calcined batch of this powder (called R/CCC BR), and the properties were found to be similar to those of the other powders.

Table 2
Comparison of the green properties of the starting powders (pellets prepared by uniaxial pressing at 250 MPa)

Alumina powders	As-received		Attrition-milled and freeze-dried	
	Density ρ (g/cm^3)	Strength σ (MPa)	Density ρ (g/cm^3)	Strength σ (MPa)
AES11C	2.28	2±0.5	2.13	6±1
P172SB	–	–	2.15	7±1
CS400M	–	–	2.10	6±1
R/CCC	2.24	29±1	2.23	30±1
R/CCC BR (calcined)	2.27	3±0.5	2.18	6±1

For the rest of the study, only the as-received and the processed AES11C and R/CCC were used in order to determine the influence of the pressing method and pressing pressure on the green density, strength and pore structure of the compacts. The effect of pressing pressure on the green density and strength are presented in Fig. 1 for uniaxially pressed pellets. In all cases, green density increased with increasing pressure. For the as-received AES11C powder, higher green density was obtained at the lower pressing pressure than for freeze-dried (FD) powder. For the R/CCC powder, there was no significant difference between the characteristics of the as-received and processed powders.

The variation in behaviour during compression and compaction of powders is usually due to differences in their particle size, and the strength and shape of the agglomerates formed. Bortzmeyer[17] has shown that the green strength of compacts prepared with powders having sizes in the range 0.2–1.5 μm increases as particle size decreases. The attrition milling of the four powders in this study reduces their particle size and thus explains partially the differences observed between the properties of as-received and freeze-dried powders. A second, and probably more significant contribution results from a change in the characteristics of the agglomerates due to freeze-drying. Indeed, in the case of spray-dried granules, for example, it has been shown that the stronger the granules (or agglomerates), the higher the green strength[18] and the lower the green density of the compacts (especially at low pressures). The as-received AES11C contained loose spherical agglomerates and the freeze-drying process caused the formation of stronger agglomerates with a flake shape as shown in Fig. 2. This difference in shape and strength of the agglomerates can thus result in differences in compression and compaction behaviour for

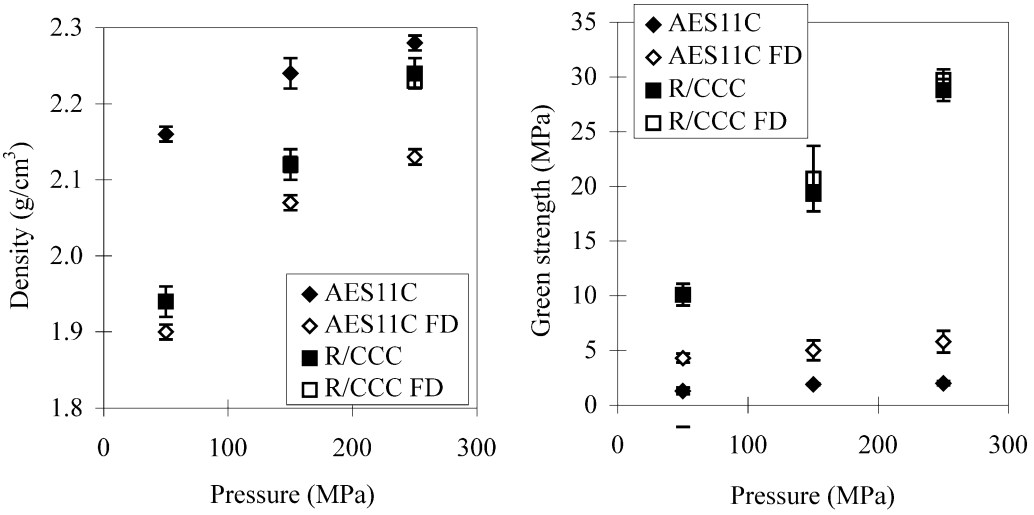

Fig. 1. Effect of of the pressing pressure on the green density and strength of compacts prepared by uniaxial pressing.

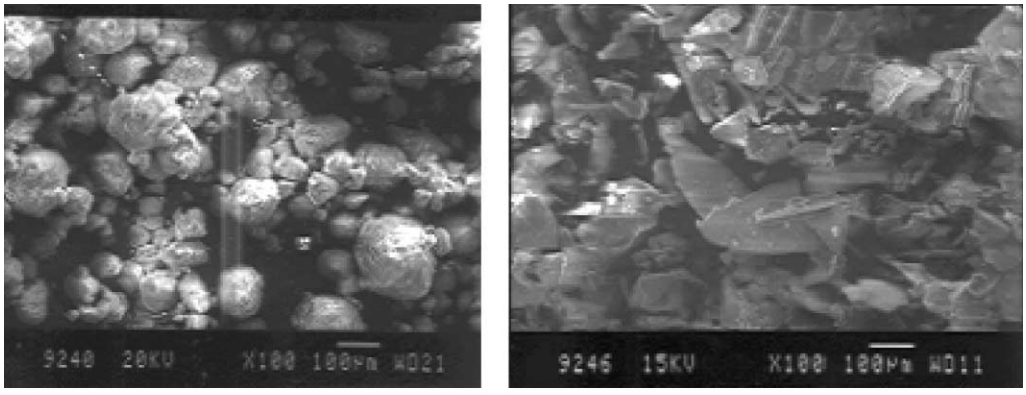

(a) As-received powder (b) Freeze-dried powder

Fig. 2. Comparison of as-received and as-freeze-dried AES11C powders (SEM observation).

as-received and processed AES11C. In the case of R/CCC, the influence of the binder on the strength of the agglomerates is predominant and no difference in behaviour between the as-received and processed powders was observed. Due to the presence of this binder, the compacts exhibited a much higher green strength than those prepared from AES11C.

A similar study conducted on pellets uniaxially pressed at 50 MPa and subsequently cold isostatically pressed between 50 and 200 MPa showed the same trends. Higher values of green density and strength were obtained especially in the absence of binder (AES11C). Cold isostatic pressing gave better results than uniaxial pressing because of the better homogeneity of the density in the compact. Indeed, for uniaxial pressing, factors such as the friction of the powder against the walls of the die during the pressing process will lead to stresses resulting in less homogeneous packing and green density.

For this reason, the pore structure of the powders was assessed on compacts prepared by cold isostatic pressing. All the powders used in this experiment exhibited a major pore population in the range 80–120 nm with a relatively narrow distribution (Fig. 3). The main difference between AES11C and R/CCC is the presence, in the latter case, of a small population of pores in the range 100–300 nm. The aqueous processing and freeze-drying leads to a slight reduction of the pore size, probably due to the reduction of the size of the particles during attrition milling. The two pore populations present in the compacts prepared from R/CCC powder can be attributed to the inter- and intra-agglomerate pores. Indeed, in this case the presence of a binder leads to the formation of harder agglomerates that are not totally "broken down" during pressing. The use of higher pressing pressures (up to 150 MPa) led to a reduction of the pore size but the pore population corresponding to inter-agglomerate pores in

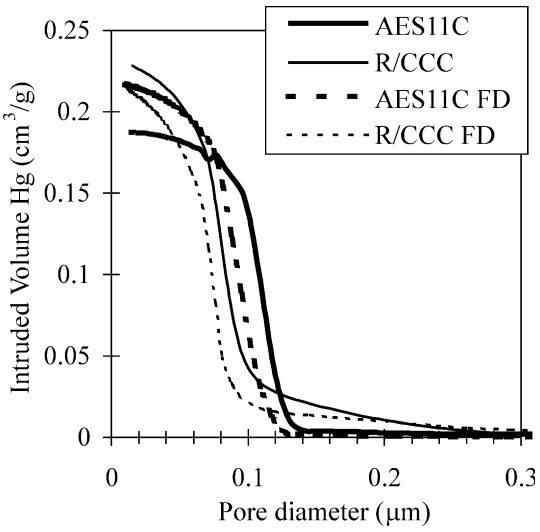

Fig. 3. Pore size distribution measured by mercury porosimetry on samples cold isostatically pressed at 50 MPa.

the R/CCC compacts were still present. These results are consistent with previous studies conducted on two similar types of powders.[17]

4.2. Sintering behaviour and microstructure

A mercury porosimetry study was conducted in order to follow the dependence of the pore structures of compacts prepared from as-received and processed AES11C (FD) and R/CCC powders at temperatures of 1200 and 1400 °C (below normal sintering temperature). One nanocomposite (AES11C-5 vol.% SiC) was also studied following heat treatment in the range 1200–1600 °C. Table 3 and Fig. 4 give the values of density, pore volume and pore size distribution observed. The total pore volume is reduced as the temperature increases without any significant reduction in the pore size, while the density of the samples increase from ~2.04 g/cm^3 (52%) to 3.07 g/cm^3 (78%). In the case of AES11C, the compact prepared from the as-received powder had a significantly higher green density than the compact prepared from the processed powder (Table 3). For the processed powder, no reduction in pore volume had occurred at 1200 °C whereas, for the as-received powders, densification had already commenced at this temperature. In the case of R/CCC, the results were similar for the as-received and processed powders as expected from their similar green densities and pore structures. At 1400 °C, the residual pore volume was always higher than that of AES11C. It can be noted that only the volume fraction of pores having sizes at around 100 nm was reduced but not the volume fraction of pores having sizes in the range 100–300 nm (inter-agglomerate pores).

The introduction of SiC particles in the AES11C matrix retarded the sintering (Table 3, Fig. 4). The decrease in the pore volume starts above 1200 °C, as for the processed matrix, but at 1400 °C the reduction of the pore volume is less and to achieve densification to the same extent as the matrix requires a higher temperature still.

The comparison of the sintering behaviour at 1650–1750 °C of nanocomposites prepared from the different alumina powders (Fig. 5) shows results consistent with the mercury porosimetry study. The lowest density (~97%) was obtained for as received R/CCC containing the binder. However, the calcined R/CCC (R/CCC BR)

Table 3
Dependence of the density and the pore volume on heat treatment temperature (%td: % of the theoretical density; the pore volume is calculated from the value of the density)

Sample	Sintering treatment	Density		Pore volume (cm^3/g)	Intruded volume of mercury (cm^3/g)
		(g/cm^3)	%td		
AES11C	Green sample	2.21	55.5	0.20	0.19
	1200 °C—1 h	2.49	62.6	0.15	0.14
	1400 °C—1 h	3.13	78.6	0.07	0.06
AES11C FD	Green sample	2.02	50.7	0.24	0.22
	1200 °C—1 h	2.08	52.6	0.23	0.21
	1400 °C—1 h	2.91	73.1	0.09	0.09
AES11C	Green sample	2.01	51.0	0.24	0.22
+5 vol.% SiC	1200 °C—1 h	2.04	51.8	0.24	0.22
	1400 °C—1 h	2.47	62.7	0.15	0.13
	1600 °C—1 h	3.39	86.0	0.04	0.03
R/CCC	Green sample	2.05	51.5	0.24	0.23
	1200 °C—1 h	2.22	55.8	0.20	0.18
	1400 °C—1 h	2.84	71.4	0.10	0.09
R/CCC FD	Green sample	1.95	49.0	0.26	0.22
	1200 °C—1 h	2.11	53.0	0.22	0.19
	1400 °C—1 h	2.88	72.4	0.10	0.08

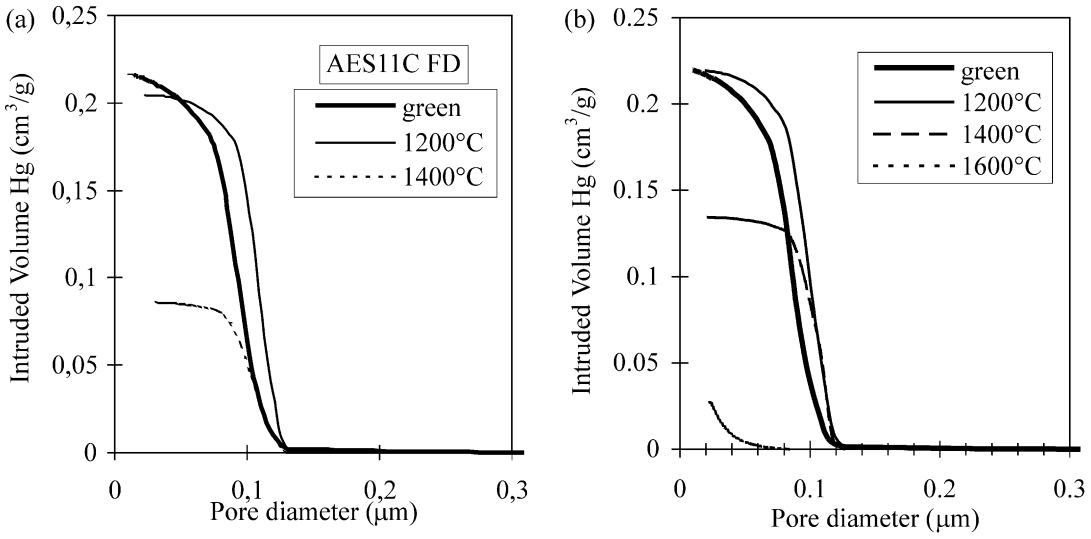

Fig. 4. Dependence of the pore size distribution of (a) processed AES11C alumina and (b) AES11C-5 vol.% SiC nanocomposite on the heat treatment temperature (green compacts obtained by CIP at 50 MPa).

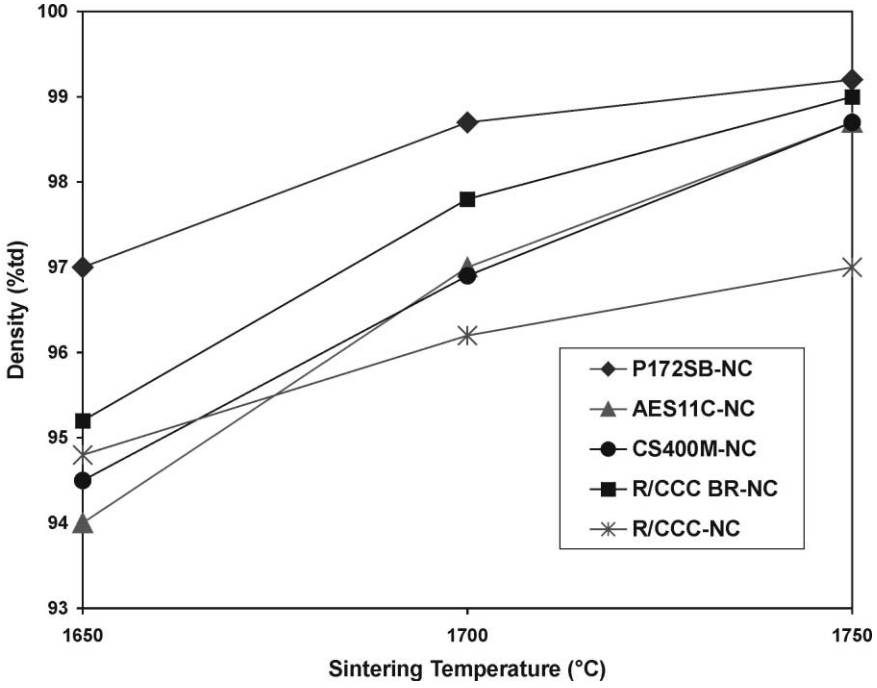

Fig. 5. Dependence of the density of nanocomposites prepared using the different alumina powders on the sintering temperature.

achieved a density of 3.90 g/cm^3 (99%) at 1750 °C. All the other materials exhibited similar densities (>98.7%) and average matrix grain size (~3 μm, Table 4) when sintered at 1750 °C. The highest values of density were obtained for nanocomposites with P172SB followed by R/CCC BR (binder removed before processing), AES11C and CS400M. These last two powders exhibited the same behaviour. The matrix microstructure of the nanocomposite produced from AES11C is more homogeneous (Fig. 6). For P172SB, a density ~99% could be obtained at 1700 °C and hence the matrix grain size was smaller (Table 4, Fig. 7). Alumina samples were sintered at 1600 and 1700 °C using as-received P172SB and their grain size was compared to the grain size obtained for the nanocomposite (Table 4). The beneficial effect of the addition of SiC on the refinement of the matrix microstructure is clear, with grain size of 2 μm compared with 13.9 μm for the monolithic alumina.

The SEM observation of the nanocomposite prepared from the as-received R/CCC powder and sintered at

Table 4
Densities and average grain size of alumina and nanocomposites sintered at different temperatures

Powder	Sintering temperature °C	Density		Matrix grain size	
		g/cm^3	%td	Average (μm)	Standard deviation
P172SB + 5 vol.% SiC	1700	3.89	98.7	2.0	0.4
P172SB + 5 vol.% SiC	1750	3.91	99.2	3.2	0.6
AES11C + 5 vol.% SiC	1750	3.89	98.7	2.8	0.2
CS400M + 5 vol.% SiC	1750	3.89	98.7	2.7	0.5
R/CCC BR + 5 vol.% SiC	1750	3.90	99.0	2.9	0.7
R/CCC + 5 vol.% SiC	1750	3.82	97.0	–	–
P172SB (alumina)	1700	3.96	99.5	13.9	2.0
P172SB (alumina)	1600	3.93	98.7	9.4	1.1

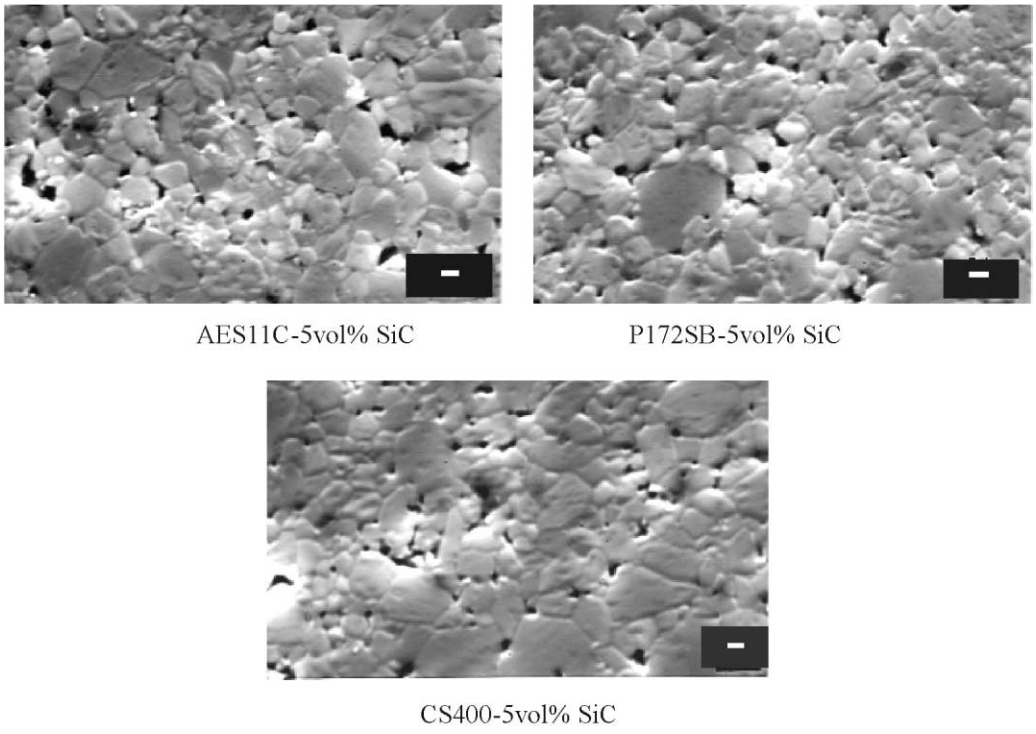

Fig. 6. Microstructure of nanocomposites prepared from AES11C, P172SB and CS400 aluminas, sintered at 1750 °C (bar = 1 μm).

1750 °C showed the presence of large elongated pores (Fig. 8). The significantly different behaviour obtained for R/CCC can be explained by the presence of inter-agglomerate pores. This population of pores is characterised by a "surface" defined by a larger number of grains. Such an arrangement is detrimental to the reduction of the pore size during sintering. This phenomenon is generally observed during sintering of compacts made from powders forming hard agglomerates and can be explained by thermodynamic considerations.[20,21] This has been reported even when the pressure used to form the green compacts was sufficient to break the agglomerates.[19] Fig. 8 shows the elongated pores observed, which certainly correspond to these remaining inter-agglomerate pores.

P172SB, AES11C, CS400 alumina powders and the calcined R/CCC (R/CCC BR) showed relatively similar sintering behaviours and microstructures even though some differences were observed. These four powders had very similar green densities, and, therefore, this parameter cannot explain these differences. AES11C and CS400M contained the lowest amount of impurities probably explaining their lower sinterability compared to P172SB and calcined R/CCC. As debonded R/CCC contained the highest amount of impurities, the best sinterability was expected. However, R/CCC had lower density than P172SB, which may be due to the difference in the respective amounts of the various impurities. A hypothesis is the high content of SiO_2 for R/CCC. Some studies have shown that this impurity can inhibit the densification of Al_2O_3.[22,23]

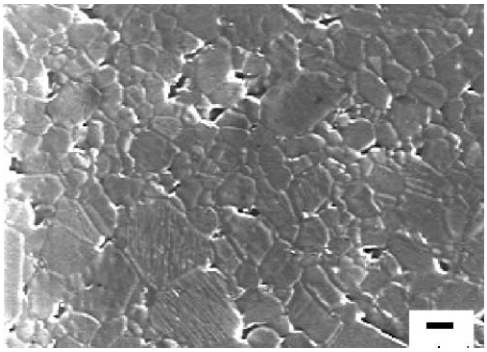

Fig. 7. Microstructure of the nanocomposite prepared from P172SB alumina sintered at 1700 °C (bar = 1 μm).

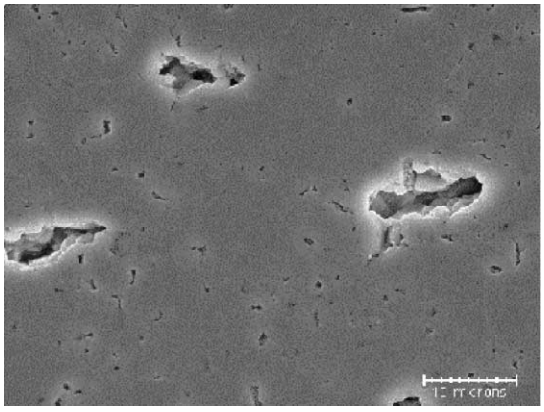

Fig. 8. SEM observation of the nanocomposite prepared from the R/CCC alumina powder and sintered at 1750 °C.

It is difficult to explain clearly the better homogeneity in microstructure obtained for AES11C. In the materials prepared here, two factors can influence abnormal grain growth.

(i) Abnormal grain growth is known to occur in Al_2O_3 during sintering at temperatures greater than 1550 °C. It can be further enhanced by inhomogeneous dispersion of impurities such as SiO_2 and CaO.[24,25]
(ii) When small particles of SiC are present, grain growth is inhibited but abnormal grain growth has already been observed in regions of these types of nanocomposites containing particles having diameters lower than 200 nm.[26] These particles are more often found in intragranular positions whereas bigger particles are more efficient in pinning grain boundaries and are usually found in intergranular positions.

As expected and reported in previous studies,[3,26,27,28] the introduction of SiC particles inhibits densification. The SiC particles are inert at these temperatures and pin the Al_2O_3 grain boundaries. The grain boundary pinning severely inhibits the grain growth leading to a decrease in densification rate. This is illustrated by the mercury porosimetry results obtained. The densification process commences for both the processed AES11C alumina and the AES11C + 5 vol.% SiC composite at a similar temperature (above 1200 °C), but the densification rate is lower for the composite (Table 3 and Fig. 4). The inhibition of grain growth is clearly illustrated here by the difference of grain size obtained in the P172SB matrix and in the composite (Table 4).

Since, it was realized very recently that UF45 SiC powder was no longer commercially available, another silicon carbide powder (UF25, Starck, Germany) was used with P172SB alumina to prepare an alumina-5 vol.% SiC nanocomposite, following the same procedure described above, in order to study the sinterability. It was found that P172SB-5 vol.% UF25 nanocomposite yielded a density value of 3.87 g/cm^3 at 1700 °C for 2 h compared to P172SB-5 vol.% UF45, which yielded 3.89 g/cm^3 at the same temperature. The slightly lower density for the nanocomposite with UF25 could be due to its lower impurity levels (free Si = 0.14 wt.%) compared to UF45 (free Si = 0.22 wt.%). This demonstrates that similar densification can be effected using different nanophase SiC powder in alumina.

4.3. Properties of the nanocomposites

The properties of the samples sintered at 1750 °C and of the composites prepared from P172SB and sintered at 1700 °C were evaluated (Table 5). All the samples,

Table 5
Elasticity, hardness and fracture toughness of the Al_2O_3–5 vol.% SiC nanocomposites

Samples	Density		Elastic properties			Hardness	Fracture toughness
	g/cm^3	%td	E (GPa)	G (GPa)	ν	(GPa)	(MPa.$\sqrt{}$m)
P172SB + 5 vol.% SiC (1700 °C)	3.89	98.7	395	159	0.24	17.6	3.0
P172SB + 5 vol.% SiC (1750 °C)	3.91	99.2	406	164	0.23	17.4	3.0
AES11C + 5 vol.% SiC (1700 °C)	3.83	97.2	–	–	–	–	–
AES11C + 5 vol.% SiC (1750 °C)	3.89	98.7	399	161	0.24	17.7	3.1
CS400M + 5 vol.% SiC (1750 °C)	3.89	98.7	397	161	0.24	17.9	3.3
R/CCC BR + 5 vol.% SiC (1750 °C)	3.90	99.0	398	160	0.24	17.7	3.0
R/CCC + 5 vol.% SiC (1750 °C)	3.82	97.0	360	146	0.23	15.2	–

except the one prepared from R/CCC, which was less dense, exhibited similar properties. Their slight differences in density or microstructure were not sufficient to cause significant impact on the properties studied here.

The Young's modulus and hardness values are similar to the values predicted by a rule of mixtures (404 and 17.5 GPa, respectively) and measured, for example, by Nakahira and Niihara.[29] Anya and Roberts[30] and Zhao et al.[31] found slightly higher hardness values.

The fracture toughness values were similar to previously reported results (for example, Anya and Roberts[30] and Zhao et al.[31]) if the same equation[31] is used for the calculations. Anya and Roberts have shown that Al_2O_3–SiC nanocomposites exhibited a Palmqvist crack system.[30] The Evans and Charles equation used in this study is, thus, not rigorously valid but it is useful for comparison of materials. Furthermore, it gives results which are closer to the values measured by other techniques such as Hertzian indentation[30] or SENB[7] on similar nanocomposites.

5. Conclusions

It is possible to produce dense Al_2O_3–SiC nanocomposites using a conventional processing route involving water processing and pressureless sintering at 1700–1750 °C.

The choice of the starting alumina powder can have a significant influence on the sinterability and the microstructure of the composite. The presence of a binder (PVA) during green processing was found to be detrimental to the sintering behaviour because it resulted in residual hard agglomerates and the accompanying inter-agglomerate pores. The highest densities were obtained with Pechiney P172SB alumina. The composites containing 5 vol.% SiC prepared with this powder could be sintered to ~99% density at 1700 °C leading to a finer matrix microstructure with mean grain size of ~2 μm compared with 13.9 μm for a monolithic alumina prepared under identical conditions. Thus, fabrication of Al_2O_3–SiC nanocomposites can be carried out using conventional processing and without the need for highly expensive, ultra fine, high purity alumina powders.

Acknowledgements

Financial support of the work under Brite-Euram Contracts CT 960212 and CT 975067 of the European Commission is gratefully acknowledged. We wish to thank our colleagues Dr. David O'Sullivan, Materials Ireland, Limerick, Dr. S. Roberts, University of Oxford, Dr. Francis Cambier, Belgian Ceramic Research Centre, Mons, Professor A. Leriche, CRITT, Maubeuge, France and Professor M. Pomeroy, University of Limerick, for useful discussions.

References

1. Niihara, K., New design concept of structural ceramics—ceramic nanocomposites. *J. Ceram. Soc. Jpn*., 1991, **99**, 974–982.
2. Niihara, K. and Nakahira, A., Structural ceramic nanocomposites by sintering method: roles of nano-size particles. In *Ceramics Towards the 21st Century*. The Ceram. Soc. of Japan, 1991, pp. 404–417.
3. Stearns, L. C., Zhao, J. and Harmer, M. P., Processing and microstructure development in Al_2O_3–SiC nanocomposites. *J. Eur. Ceram. Soc*., 1992, **10**, 473–477.
4. Borsa, C. E., Jiao, S., Todd, R. I. and Brook, R. J., Processing and properties of Al_2O_3/SiC nanocomposites. *J. Microscopy*, 1994, **177**, 305–312.
5. Sternitzcke, M., Review: structural ceramic nanocomposites. *J. Eur. Ceram. Soc*., 1997, **17**, 1061–1082.
6. Zhao, J., Stearns, L. C., Harmer, M. P., Chan, H. M. and Miller, G. A., Mechanical behaviour of alumina-silicon carbide nanocomposites. *J. Am. Ceram. Soc*., 1993, **76**(2), 503–510.
7. Davidge, R. W., Brook, R. J., Cambier, F., Poorteman, M., Leriche, A., O'Sullivan, D., Hampshire, S. and Kennedy, T., Fabrication, properties and modelling of engineering ceramics reinforced with nanoparticles of silicon carbide. *Br. Ceram. Trans*., 1997, **96**(3), 121–127.
8. Kennedy, T., Brown, J., Doyle, J. and Hampshire, S., Oxidation behavior and high temperature strength of alumina-silicon carbide nanocomposites. In *Corrosion of Advanced Ceramics, Key Engineering Materials*, Vol. 113, ed. R. J. Fordham, D. J. Baxter and T. Graziani. Trans Tech Publications, 1996, pp. 65–70.
9. Davidge, R. W., Twigg, P. C. and Riley, F. L., Effects of silicon carbide nano-phase on the wet erosive wear of polycrystalline alumina. *J. Eur. Ceram. Soc*., 1996, **16**, 799–802.
10. Anya, C. C. and Roberts, S., Pressureless sintering and elastic constants of Al_2O_3–SiC nanocomposites. *J. Eur. Ceram. Soc*., 1997, **17**, 565–573.
11. Ohji, T., Nakahira, A., Hirano, T. and Niihara, K., Tensile creep behaviour of alumina/silicon carbide nanocomposite. *J. Am. Ceram. Soc*., 1994, **12**, 3259–3262.
12. Thompson, A. M., Chan, H. M. and Harmer, M. P., Tensile creep of alumina-silicon carbide nanocomposites. *J. Am. Ceram. Soc*., 1977, **9**, 2221–2228.
13. Descamps, P., O'Sullivan, D., Poorteman, M., Descamps, J. C., Leriche, A. and Cambier, F., Creep behaviour of Al_2O_3–SiC nanocomposites. *J. Eur. Ceram. Soc*., 1999, **19**, 2475–2485.
14. O'Sullivan, D., Poorteman, M., Therry, B., Leriche, A., Descamps, P. and Cambier, F., Comparison of properties of alumina-silicon carbide nanocomposites processed in aqueous and organic media. *Silicates Industriels*, 1996, **11–12**, 235–241.
15. Wurst, J. C. and Nelson, J. A., Linear intercept technique for measuring grain size in two-phase polycrystalline ceramics. *J. Am. Ceram. Soc*., 1972, **55**(2), 109.
16. Evans, A. G. and Charles, E. A., *J. Am. Ceram. Soc*., 1976, **59**(7-8), 371–372.
17. Bortzmeyer, B., Tensile strength of ceramic powders. *J. Mater. Sci*., 1992, **27**, 3305–3308.
18. Lam, D. C. C. and Kusakari, K., Microstructure and mechanical properties relations for green bodies compacted from spray-dried granules. *J. Mater. Sci*., 1995, **30**, 5495–5501.
19. Welker, M. and Hausner, H., Agglomerate characteristics and sintering behavior of alumina powders. *CFI/Ber. DKG*, 1992, **69**(9), 318–325.
20. Kingery, W. D. and Francois, B., *Sintering and Related Phenomena*. Gordon and Breach, New York, 1967.
21. Kellet, B. J. and Lange, F. F., Thermodynamics of densification: I. Sintering of simple particle arrays, equilibrium configurations, pore stability and shrinkage. *J. Am. Ceram. Soc*., 1989, **72**, 725–734.

22. Sumita, S., Influence of oxide additives, firing temperature, and dispersing media on sintered Al_2O_3. *Nippon Seramikkusu Kyokai Gakujutsu Rombunshi*, 1991, **99**(7), 538–544.
23. Sumita, S. and Bowen, H. K., Effect of foreign oxides on grain growth and densification of sintered alumina. In *Ceramic Transactions; Ceramic Powder Science II*, ed. G. L. Messing, E. R. Fuller and H. Hausner. American Ceramic Society, Westerville, OH, 1988, pp. 840–847.
24. Handwerker, C. A., Morris, P. A. and Coble, R. L., Effects of chemical inhomogenities on grain growth and microstructure in Al_2O_3. *J. Am. Ceram. Soc.*, 1989, **72**(1), 130–136.
25. Bae, I. and Baik, S., Abnormal grain growth of alumina. *J. Am. Ceram. Soc.*, 1997, **80**(5), 1149–1156.
26. Xu, Y., Zangvil, A. and Kerber, A., SiC nanoparticle-reinforced Al_2O_3 matrix composites: role of intra- and intergranular particles. *J. Eur. Ceram. Soc.*, 1997, **17**, 921–928.
27. Jang, H. M., Rhine, W. E. and Bowen, H. K., Densification of alumina-silicon carbide powder composites: II, Microstructural evolution and densification. *J. Am. Ceram. Soc.*, 1989, **72**(6), 954–958.
28. Piciacchio, A., Lee, S. and Messing, G. L., Processing and microstructure development in alumina-silicon carbide intergranular particulate composites. *J. Am. Ceram. Soc.*, 1994, **77**(8), 2157–2164.
29. Nakahira, A. and Niihara, K., Microstructures and fracture behaviors at high temperatures for Al_2O_3–SiC nanocomposites. In *Fracture Mechanics of Ceramics,* Vol. 9, ed. R. C. Bradt. Plenum Press, New York, 1992, pp. 165–178.
30. Anya, C. C. and Roberts, S. G., Indentation fracture toughness and surface flaw analysis of sintered alumina/SiC nanocomposites. *J. Eur. Ceram. Soc.*, 1996, **16**, 1107–1114.
31. Zhao, J., Stearns, L. C., Harmer, M. P., Chan, H. M. and Miller, G. A., Mechanical behavior of alumina-silicon carbide nanocomposites. *J. Am. Ceram. Soc.*, 1995, **76**(2), 503–510.